Supporting Information

Affinity proteomics reveals elevated muscle proteins in plasma of children with cerebral malaria

Julie Bachmann[1#], Florence Burté[2#], Setia Pramana[3], Ianina Conte[2], Biobele J. Brown[4,5,6], Adebola E. Orimadegun[3], Wasiu A. Ajetunmobi[4], Nathaniel K. Afolabi[4], Francis Akinkunmi[4], Samuel Omokhodion[4,6], Felix O. Akinbami[4,6], Wuraola A. Shokunbi[5,6], Caroline Kampf[7], Yudi Pawitan[3], Mathias Uhlén[1], Olugbemiro Sodeinde[2,4,5,6], Jochen M. Schwenk[1], Mats Wahlgren[8*], Delmiro Fernandez-Reyes[2,4,5,6*], Peter Nilsson[1*]

Legends to Supplementary Information

Figure S1. Intra-assay and inter-assay variance of suspension bead array. A) To analyze the intra-assay variance of one multiplex array, the coefficient of variation (CV) of each antibody (k=384) was determined in sample replicates (n=24) of one array experiment. 350 antibodies showed a CV of <10% and only 2 antibodies were >20%. B) The technical inter-assay variance was evaluated by comparing sample-wise and antibody-wise correlations of two independently performed array experiments. The Spearman correlation coefficient between each duplicated sample was *rho*<0.94. Antibodies in two independent arrays showed a median Spearman *rho*=0.88 ranging between 0.45 and 0.99. In both experiments two samples were excluded due to technical failure. C) Sample- and antibody-wise correlation coefficients for the 24 duplicated patient samples in discovery and verification set with the top 29 proteins.

Figure S2. A) Principal component analysis (PCA) visualizing samples of "random" and "targeted" antibody profiling (k = 384 antibodies, n = 354 samples). B) Principal component analysis (PCA) of samples with the top significant 29 proteins from the "targeted array" (k = 29 antibodies, n = 354 samples). Three-dimensional plots based on the first three dimensions of the PCA results are presented. All samples are colored based on the respective group affiliation. C) Heatmap showing protein profiles of the identified 29 host proteins. Samples were clustered based on Euclidian distance using the complete linkage method for hierarchical clustering. Proteins were sorted according to SOTA clusters. CC = grey, UM = green, SMA = red, CM = blue.

Figure S3. Correlations and boxplots of the 29 identified discriminatory proteins from the 'targeted array'. The discovery screening using the 'targeted array' was performed in two independent experiments. For each of the 29 significant proteins corresponding correlations with the Spearman coefficient (*rho)* and boxplots from experiment 1 (Exp1) and

the replicated experiment 2 (Exp2) are represented. All antibodies with significant differences showed *rho*>0.8.

Figure S4. Boxplots of the identified proteins from the 'random arrays'. Aiming at the identification of new proteins that have not been described in the context of malaria before, a part of the discovery screening was performed using 'random arrays'. These were created using a random selection of 760 antibodies being compiled from the collection of validated antibodies within HPA. Applying a non-parametric test (Kruskal-Wallis), 12 proteins were identified showing significant differences ($p<0.001$) between at least two of the four groups. ADSSL1 = adenylosuccinate synthase-like 1, CEBPA = CCAAT/enhancer binding protein (C/EBP)/ alpha, FAM71F2 = family with sequence similarity 71/ member F2, MSRB1 = methionine sulfoxide reductase B1, HAP1 = huntingtin-associated protein 1, DAPK1 = death-associated protein kinase 1, DNPEP = aspartyl aminopeptidase, MYO15A = myosin XVA, CCDC102A = coiled-coil domain containing 102A, SEC24C = SEC24 family, EEF2 = eukaryotic translation elongation factor 2, TIPIN = TIMELESS interacting protein.

Figure S5. Single proteins with significant differences between the three malaria disease groups. For pairwise comparisons of the groups, Wilcoxon rank sum test was applied (with continuity correction). A volcano plot displaying the relationship between the fold-change and significance was generated. Proteins with a p-value $< 0.1^{-6}$ (corresponds to Bonferroni adjusted p-value < 0.001) are displayed in red. See Table S1 in Text S1 for further details.

Figure S6. Technical verification of multivariate model and variable selection refinement. A) Area under ROC curve (AUC) of identified combinatory panels using the technical replicate data set in the discovery phase. For a first verification of the identified multi-protein signatures, the parameter estimates from the first dataset were used to obtain the prediction based on the second replicate data of the discovery cohort. B) Variable selection refinement. In order to investigate, which proteins contribute predominantly to the classification performance, the classifiers were sorted based on their absolute parameters obtained from L1-penalized logistic model. The logistic models of top *k* proteins were fitted and the AUC was calculated for each model. The effect on the classification performance of including the proteins is represented by the improvement of the AUC (see also Table S2 in Text S2).

Figure S7. Boxplots of CA3, CK and VWF analyzed with different antibodies in the discovery and the verification set. Various antibodies generated against different antigen sequences were used to validate the protein profile of (A) CA3, (B) CK and (C) VWF in the discovery and in the verification cohort. CA3: Carbonic anhydrase (R&D, #AF2185), CKM:

Creatine kinase-M isoform (R&D, #MAB5564 and #G113C), vWF: von Willebrand Factor. DC = Discovery cohort, VC = Verification cohort.

Figure S8. Immunohistochemical analysis of antibodies using bright field microscopy. A) Protein expression (brown) and counterstaining (blue) of anti-CA3, -CK and -MB antibodies on healthy adult tissues is presented. All 5 antibodies showed cytoplasmic positivity in skeletal muscle. Heart muscle displayed cytoplasmic immunoreactivity with 3 out of 5 antibodies used in the study. One candidate showed negative cytoplasmic staining in CNS. B) Immunohistochemical analysis of anti-VWF and anti-SERPINA3 antibodies. Most tissues showed moderate to strong immunoreactivity in blood vessels. HPA00893 lacked blood vessel positivity in heart muscle. HPA02560 showed weak positivity in heart muscle and lacked immunoreactivity in cerebellum. CK: creatine kinase; CA3: Carbonic anhydrase 3; MB: Myoglobin; VWF: von Willebrand Factor; SERPINA3: serpin peptidase inhibitor, member 3.

Figure S9. Properties of targeted antibody array. Ingenuity Pathway analysis software (Igenuity Systems) was used to identify the most important canonical pathways that were enriched in the selected antibody array compared to the Ingenuity default background. *Acute phase signaling* was enriched most significantly and is displayed. Nearly all plasma proteins that are secreted during *acute phase signaling* were covered in the targeted array (orange circles). In the SOTA cluster 'Malaria increased' (see Fig. 2) were found 6 of 46 acute phase signaling plasma proteins: CRP, LBP, ORM1, SERPINA3, TNFRSF1B and VWF (red circles).

Figure S10: Boxplots of the significant proteins and muscle proteins from the DC cohort. The verification screening using was performed in an additional group to the discovery cohort and directely compared to the CM group. The Boxplots for muscle specific proteins and significant proteins is shown .

Table S1. Univariate two-group comparisons.

Table S2. Plasma protein signatures discriminating malaria disease groups after variable selection refinement.

Table S3. Antibody-antigen properties**.**

Table S4. List of target proteins used in the targeted array

Methods S1. More detailed information regarding the procedures utilized for: Case definitions, Clinical data and sample collection, Biotinylation of plasma samples, Quality assessment of suspension bead-array, Immunohistochemistry, Self-organizing tree algorithm (SOTA) analysis, Multivariate analysis.

Supplementary Figures

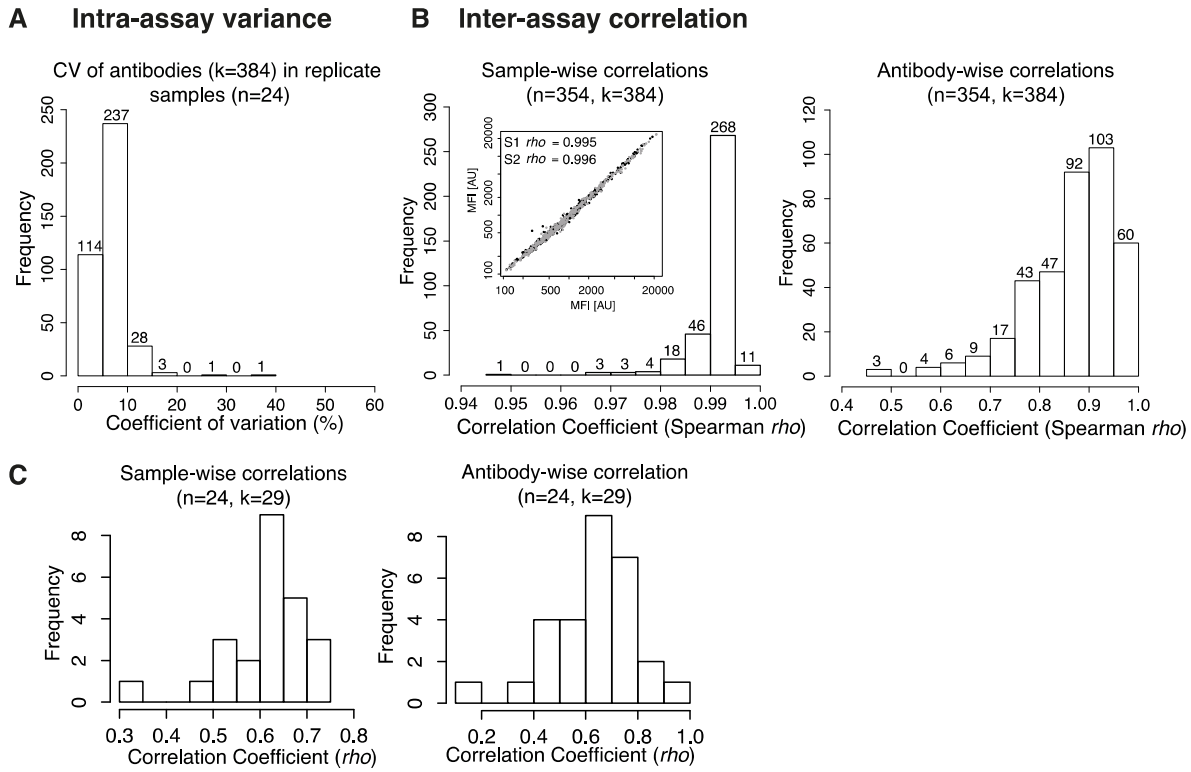

Figure S1.

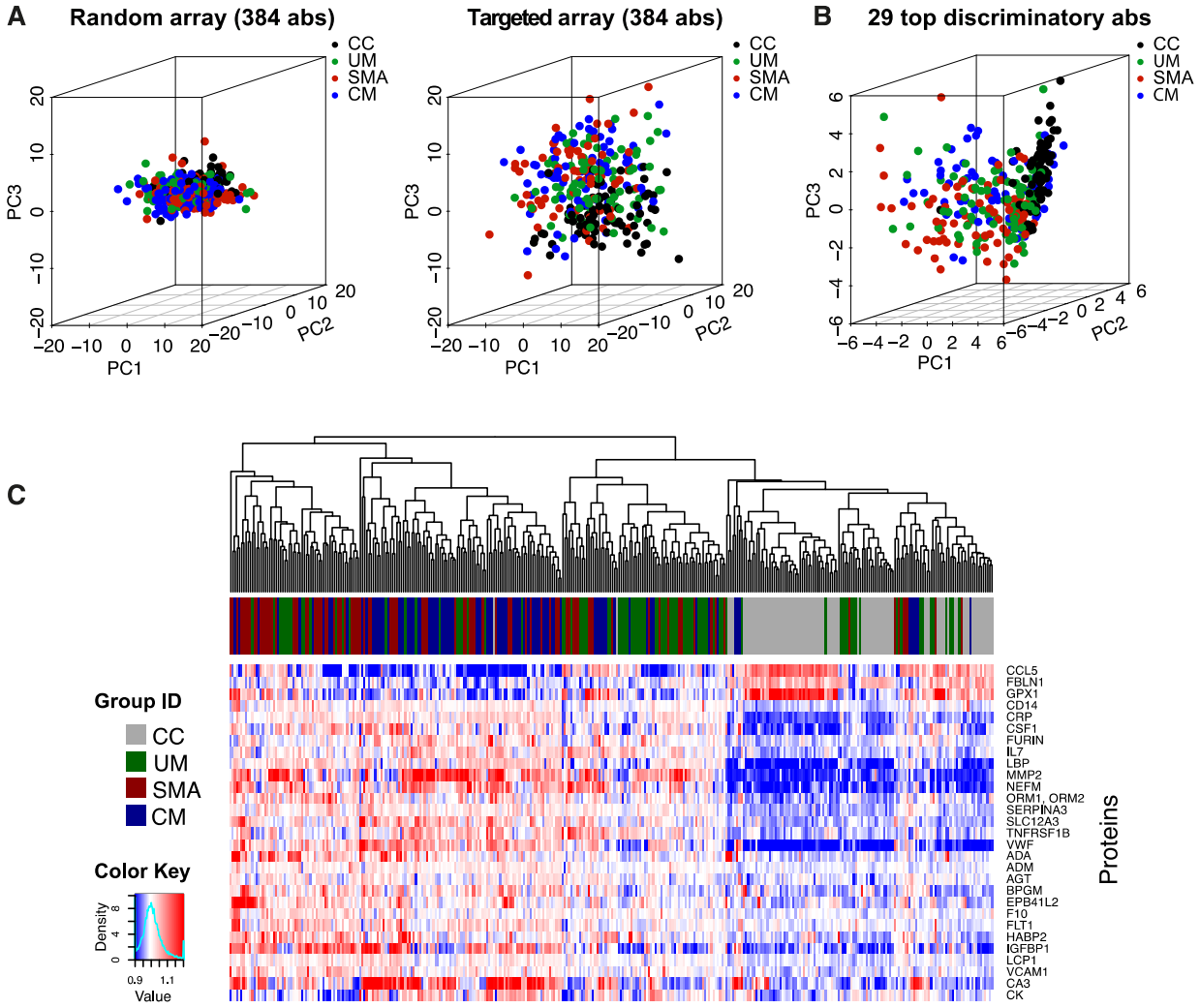
A
Random array (384 abs)
Targeted array (384 abs)
B
29 top discriminatory abs
CC
UM
SMA
CM
PC1
PC2
PC3
C
Group ID
CC
UM
SMA
CM
Color Key
Density
Value
Proteins
CCL5
FBLN1
GPX1
CD14
CRP
CSF1
FURIN
IL7
LBP
MMP2
NEFM
ORM1, ORM2
SERPINA3
SLC12A3
TNFRSF1B
VWF
ADA
ADM
AGT
BPGM
EPB41L2
F10
FLT1
HABP2
IGFBP1
LCP1
VCAM1
CA3
CK

Figure S2.

Figure S3

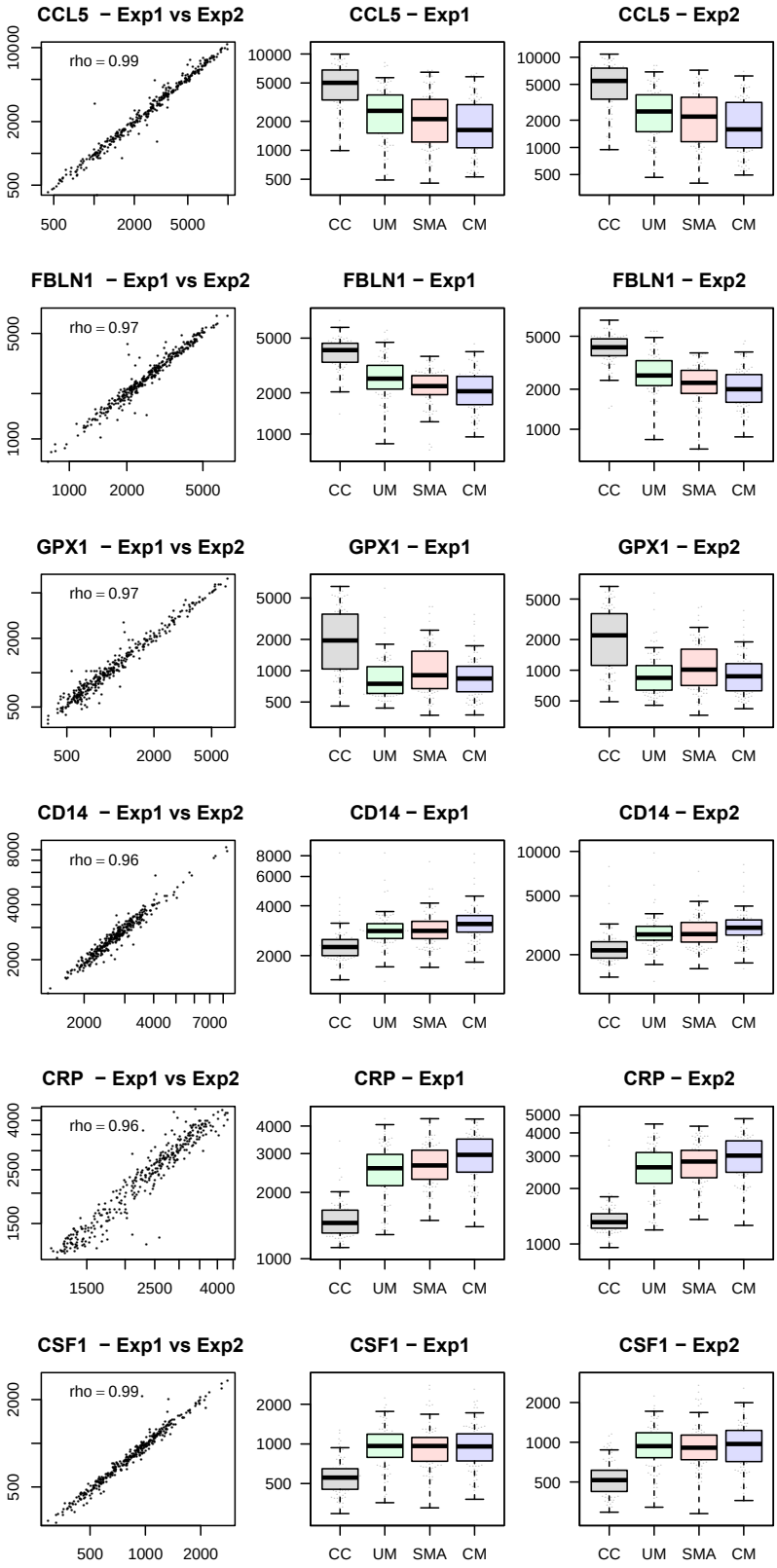
CCL5 − Exp1 vs Exp2
rho = 0.99
CCL5 − Exp1
CCL5 − Exp2
FBLN1 − Exp1 vs Exp2
rho = 0.97
FBLN1 − Exp1
FBLN1 − Exp2
GPX1 − Exp1 vs Exp2
rho = 0.97
GPX1 − Exp1
GPX1 − Exp2
CD14 − Exp1 vs Exp2
rho = 0.96
CD14 − Exp1
CD14 − Exp2
CRP − Exp1 vs Exp2
rho = 0.96
CRP − Exp1
CRP − Exp2
CSF1 − Exp1 vs Exp2
rho = 0.99
CSF1 − Exp1
CSF1 − Exp2
CC
UM
SMA
CM

Figure S3

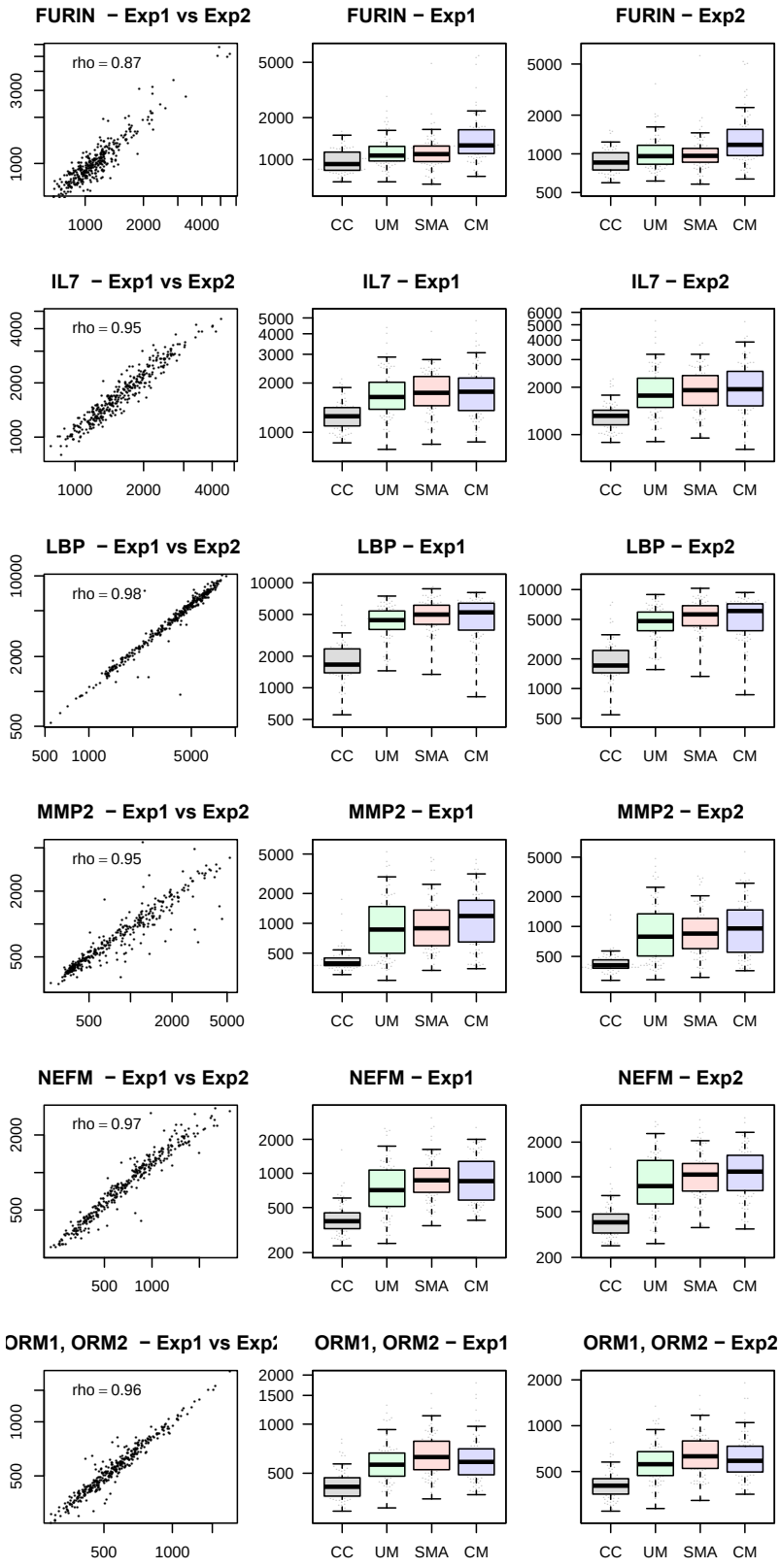
FURIN − Exp1 vs Exp2
rho = 0.87
FURIN − Exp1
FURIN − Exp2
IL7 − Exp1 vs Exp2
rho = 0.95
IL7 − Exp1
IL7 − Exp2
LBP − Exp1 vs Exp2
rho = 0.98
LBP − Exp1
LBP − Exp2
MMP2 − Exp1 vs Exp2
rho = 0.95
MMP2 − Exp1
MMP2 − Exp2
NEFM − Exp1 vs Exp2
rho = 0.97
NEFM − Exp1
NEFM − Exp2
ORM1, ORM2 − Exp1 vs Exp2
rho = 0.96
ORM1, ORM2 − Exp1
ORM1, ORM2 − Exp2
CC
UM
SMA
CM

Figure S3

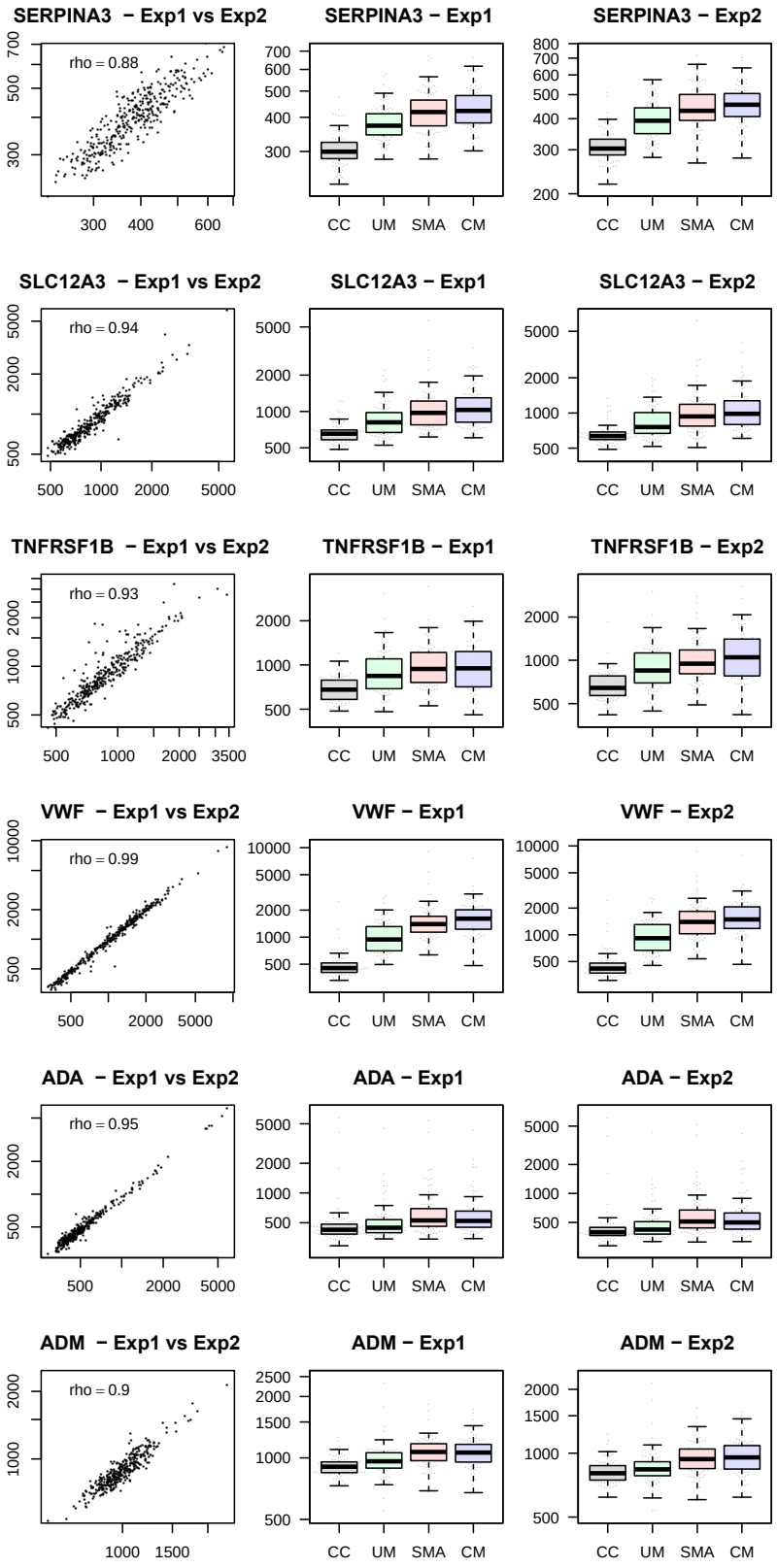
SERPINA3 − Exp1 vs Exp2
rho = 0.88
SERPINA3 − Exp1
SERPINA3 − Exp2
SLC12A3 − Exp1 vs Exp2
rho = 0.94
SLC12A3 − Exp1
SLC12A3 − Exp2
TNFRSF1B − Exp1 vs Exp2
rho = 0.93
TNFRSF1B − Exp1
TNFRSF1B − Exp2
VWF − Exp1 vs Exp2
rho = 0.99
VWF − Exp1
VWF − Exp2
ADA − Exp1 vs Exp2
rho = 0.95
ADA − Exp1
ADA − Exp2
ADM − Exp1 vs Exp2
rho = 0.9
ADM − Exp1
ADM − Exp2
CC UM SMA CM

Figure S3

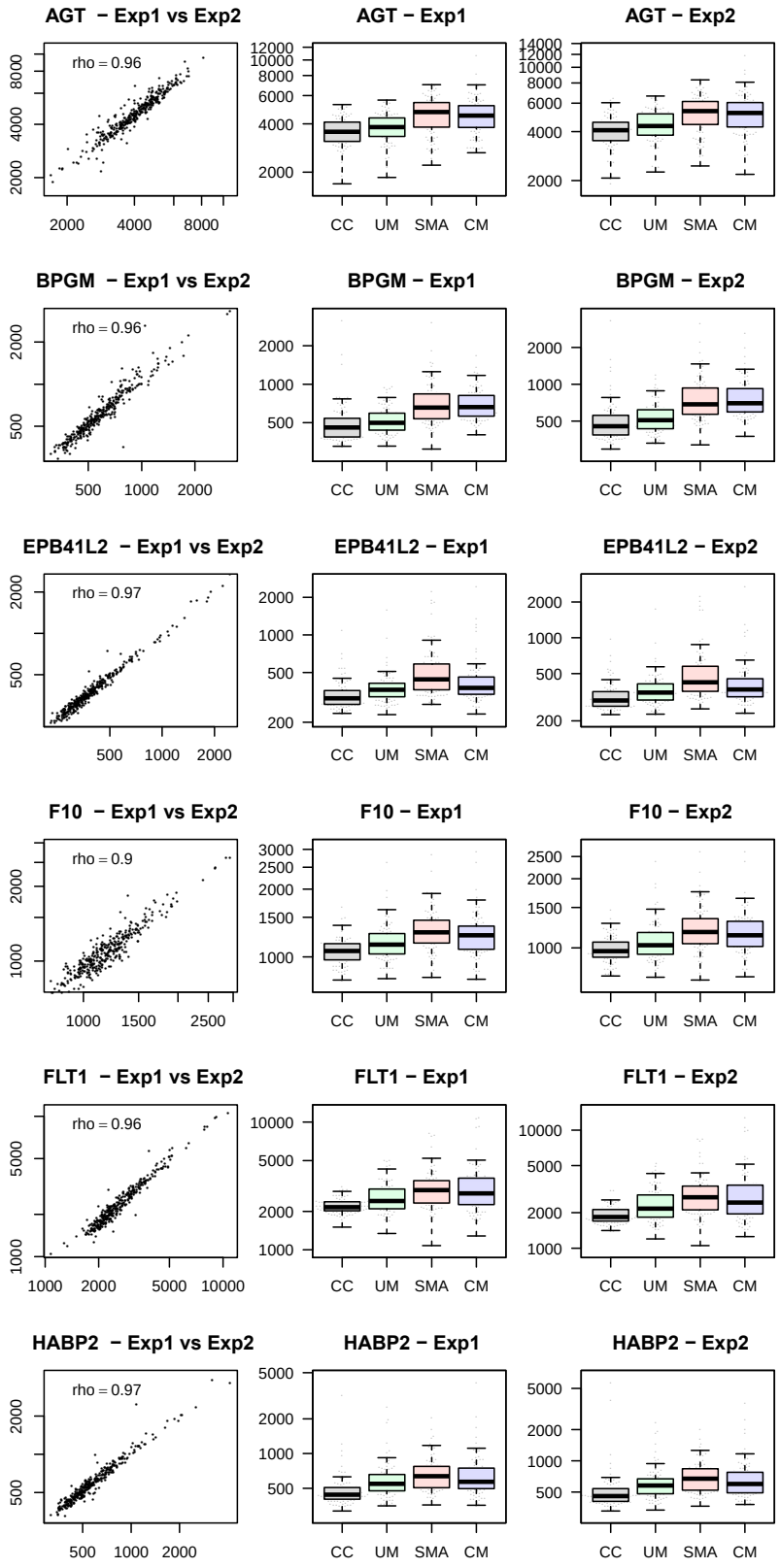
AGT − Exp1 vs Exp2
rho = 0.96
AGT − Exp1
AGT − Exp2
BPGM − Exp1 vs Exp2
rho = 0.96
BPGM − Exp1
BPGM − Exp2
EPB41L2 − Exp1 vs Exp2
rho = 0.97
EPB41L2 − Exp1
EPB41L2 − Exp2
F10 − Exp1 vs Exp2
rho = 0.9
F10 − Exp1
F10 − Exp2
FLT1 − Exp1 vs Exp2
rho = 0.96
FLT1 − Exp1
FLT1 − Exp2
HABP2 − Exp1 vs Exp2
rho = 0.97
HABP2 − Exp1
HABP2 − Exp2
CC UM SMA CM

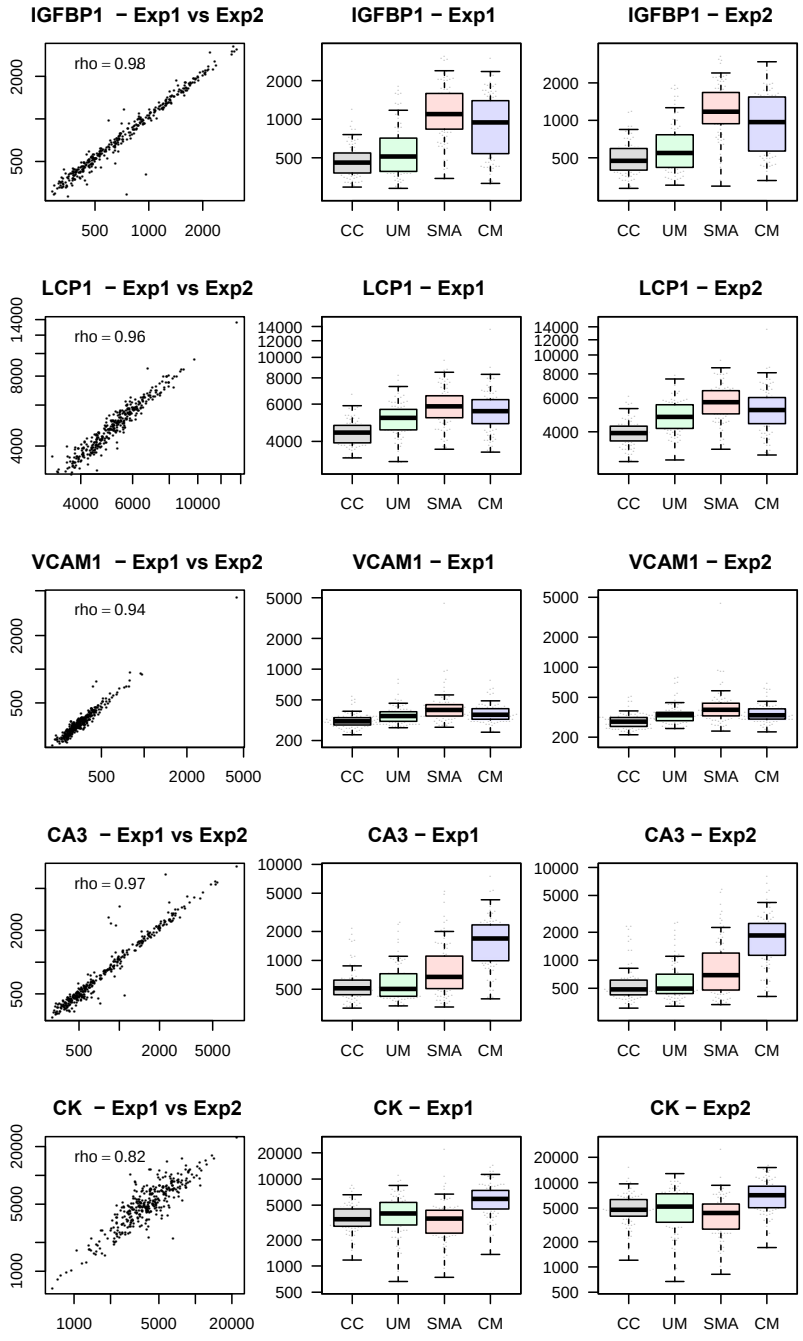
IGFBP1 − Exp1 vs Exp2
rho = 0.98
IGFBP1 − Exp1
IGFBP1 − Exp2
LCP1 − Exp1 vs Exp2
rho = 0.96
LCP1 − Exp1
LCP1 − Exp2
VCAM1 − Exp1 vs Exp2
rho = 0.94
VCAM1 − Exp1
VCAM1 − Exp2
CA3 − Exp1 vs Exp2
rho = 0.97
CA3 − Exp1
CA3 − Exp2
CK − Exp1 vs Exp2
rho = 0.82
CK − Exp1
CK − Exp2
CC
UM
SMA
CM

Figure S3.

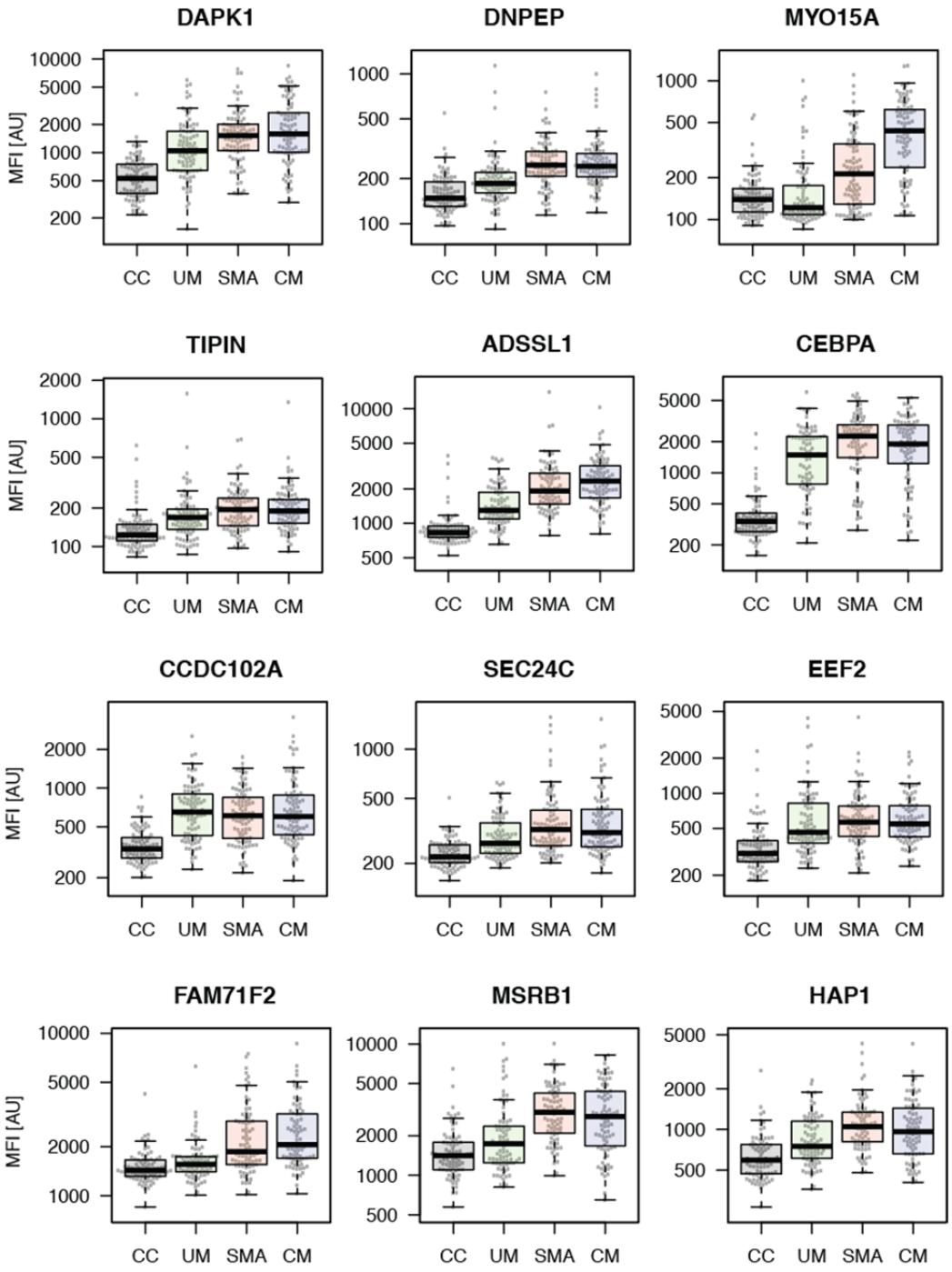
DAPK1
DNPEP
MYO15A
TIPIN
ADSSL1
CEBPA
CCDC102A
SEC24C
EEF2
FAM71F2
MSRB1
HAP1
MFI [AU]
CC
UM
SMA
CM

Figure S4.

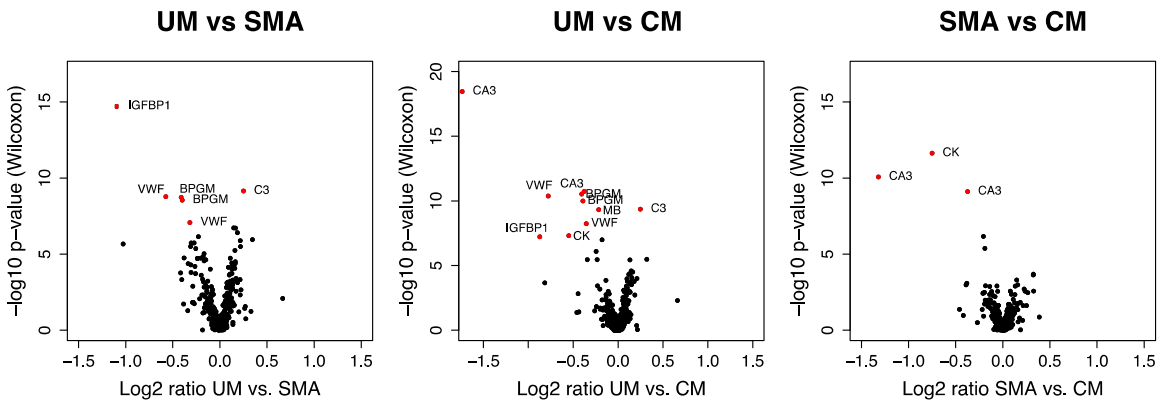
UM vs SMA
UM vs CM
SMA vs CM
−log10 p−value (Wilcoxon)
Log2 ratio UM vs. SMA
Log2 ratio UM vs. CM
Log2 ratio SMA vs. CM
IGFBP1
VWF
BPGM
C3
CA3
MB
CK

Figure S5.

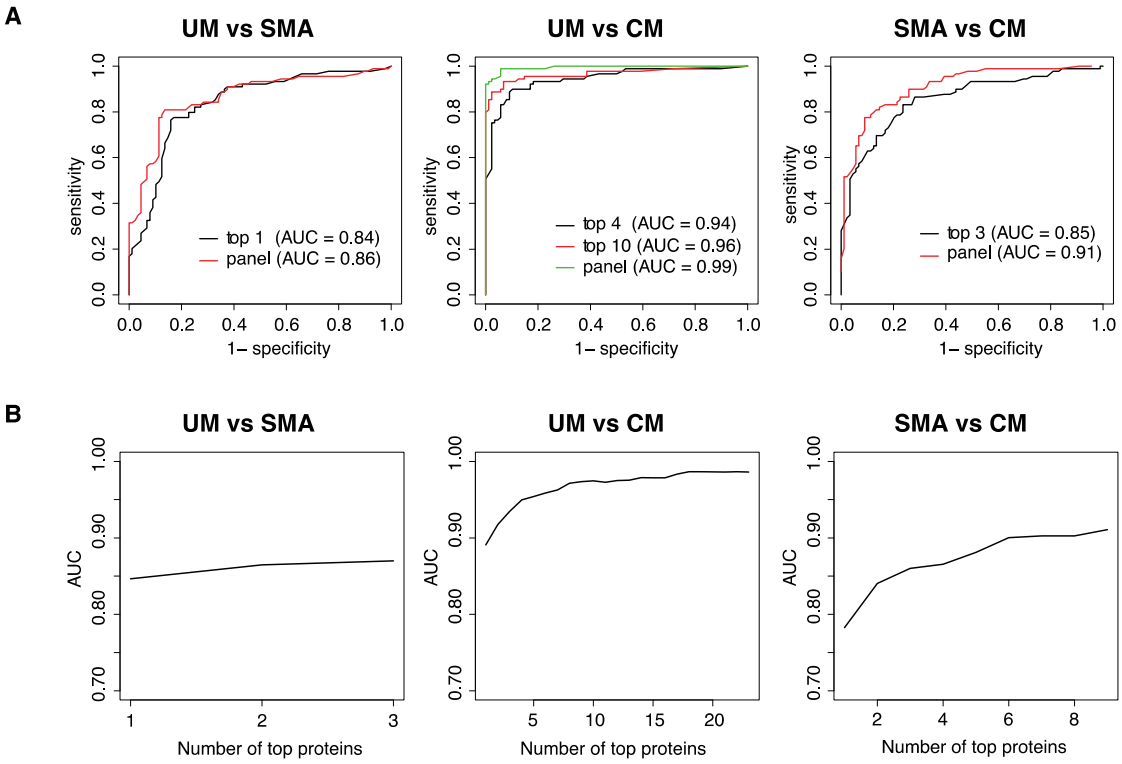
A
UM vs SMA
sensitivity
1– specificity
top 1 (AUC = 0.84)
panel (AUC = 0.86)
UM vs CM
top 4 (AUC = 0.94)
top 10 (AUC = 0.96)
panel (AUC = 0.99)
SMA vs CM
top 3 (AUC = 0.85)
panel (AUC = 0.91)
B
AUC
Number of top proteins

Figure S6.

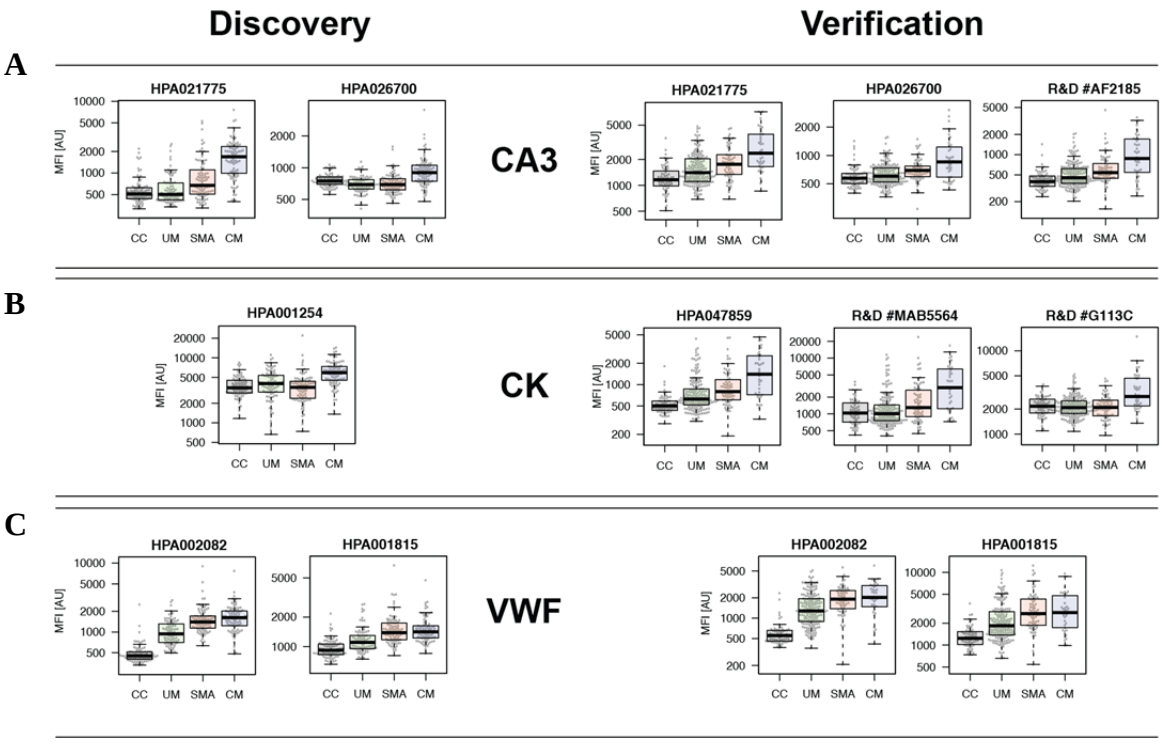
Discovery
Verification
A
HPA021775
HPA026700
HPA021775
HPA026700
R&D #AF2185
CA3
B
HPA001254
HPA047859
R&D #MAB5564
R&D #G113C
CK
C
HPA002082
HPA001815
HPA002082
HPA001815
VWF
MFI [AU]
CC UM SMA CM

Figure S7.

A

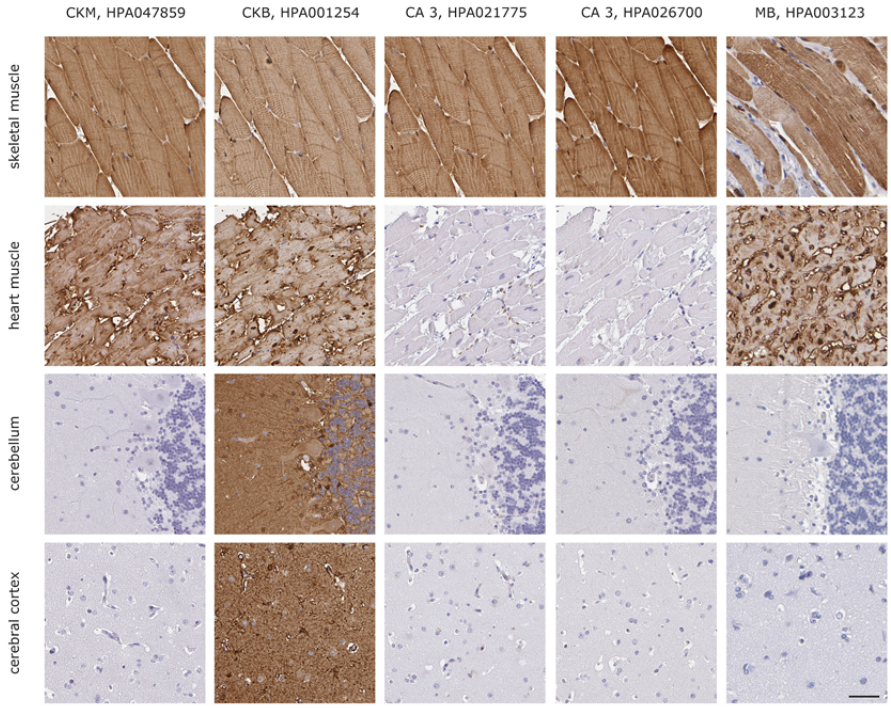
CKM, HPA047859
CKB, HPA001254
CA 3, HPA021775
CA 3, HPA026700
MB, HPA003123
skeletal muscle
heart muscle
cerebellum
cerebral cortex

B

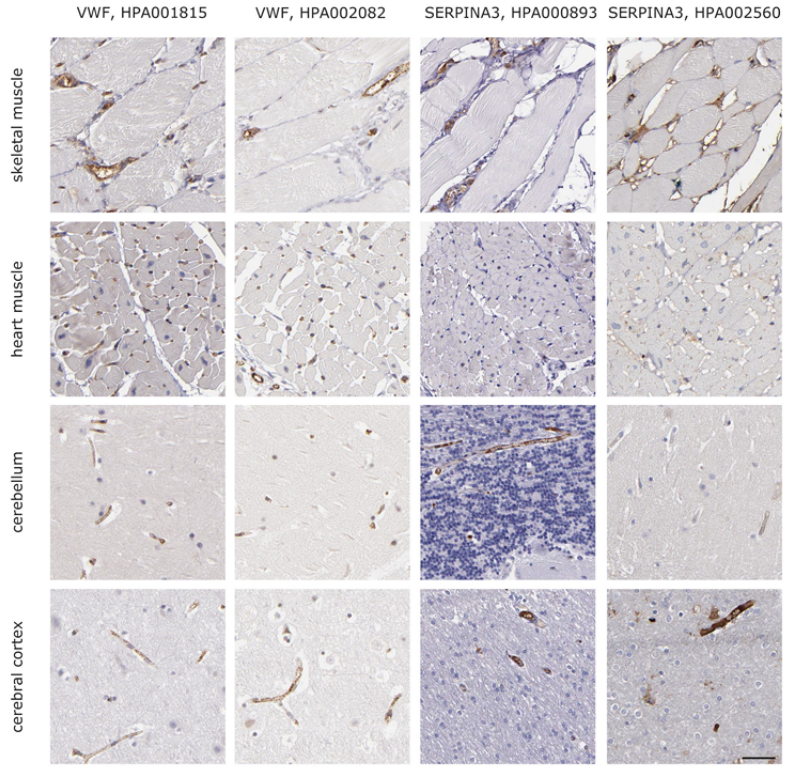
VWF, HPA001815
VWF, HPA002082
SERPINA3, HPA000893
SERPINA3, HPA002560
skeletal muscle
heart muscle
cerebellum
cerebral cortex

Figure S8.

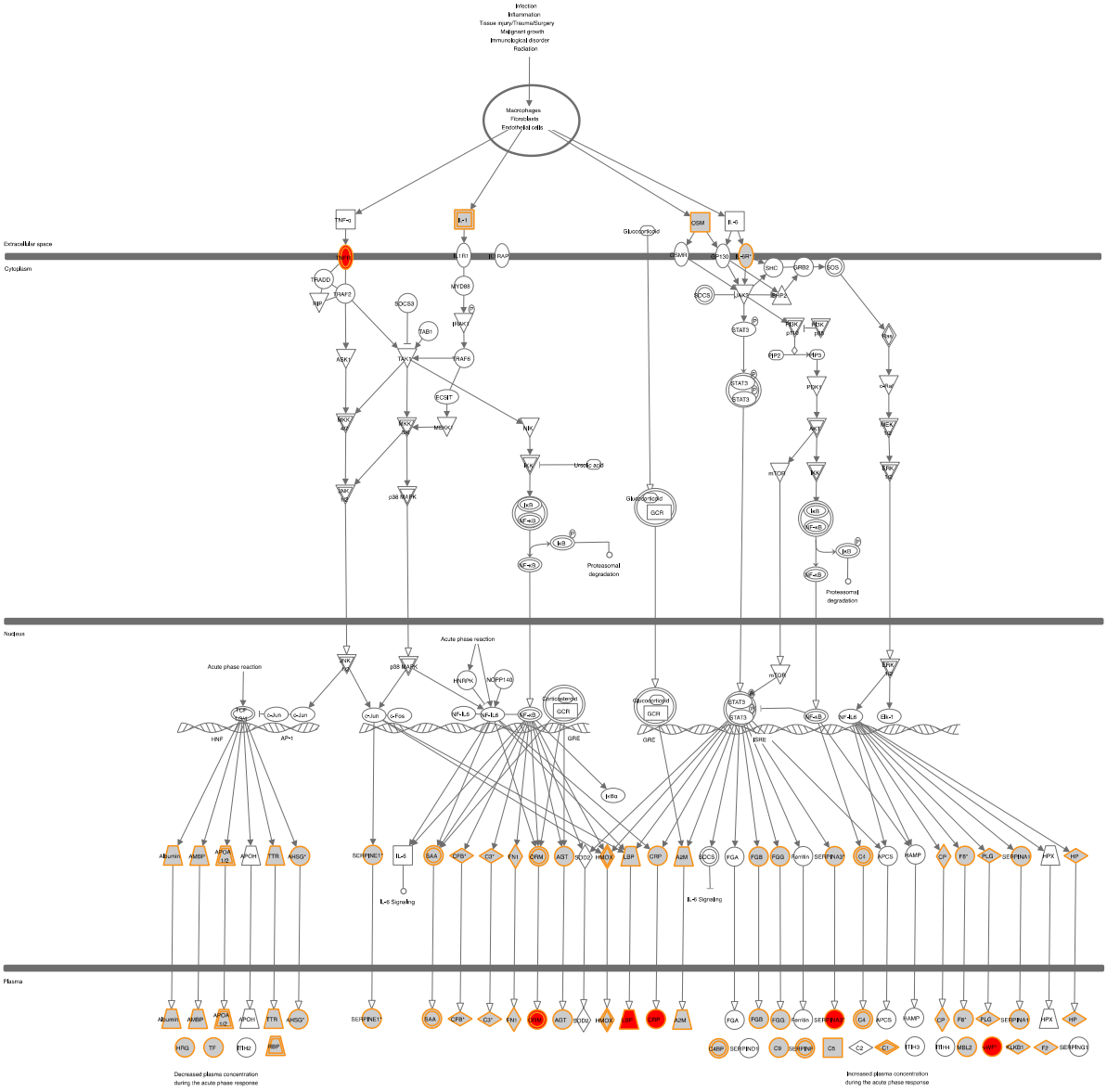
Infection
Inflammation
Tissue injury/Trauma/Surgery
Malignant growth
Immunological disorder
Radiation
Macrophages
Fibroblasts
Endothelial cells
TNF-α
IL-1
OSM
IL-6
Glucocorticoid
Extracellular space
Cytoplasm
TNFR
IL1R1
IL1RAP
OSMR
gp130
IL6R
GHC
GRB2
SOS
TRADD
TRAF2
RIP
MYD88
SOCS3
TAB1
IRAK1
ASK1
TAK1
TRAF6
ECSIT
MKK7
MKK4
MEKK1
NIK
IKK
Ursolic acid
JNK
p38 MAPK
IκB
NF-κB
Proteasomal degradation
GCR
JAK2
TYK2
STAT3
PI3K
mTOR
AKT
MEK
ERK
Nucleus
Acute phase reaction
HNF
AP-1
c-Jun
c-Fos
HNRNP
NOPP140
NF-IL6
GRE
ISRE
IκBα
Plasma
ALbumin
AMBP
APOA1/2
APOH
TTR
AHSG*
SERPINE1*
IL-6
SAA
CFB*
C3*
FN1
CRM
AGT
SOD2
HMOX
LBP
CRP
A2M
SOCS
FGA
FGB
FGG
Ferritin
SERPINA3
C4
APCS
HAMP
CP
FB*
PLG
SERPINA1
HPX
HP
IL-6 Signaling
HRG
TF
ITIH2
ITIH4
MBL2
KLKB1
F2
SERPING1
C4BP
SERPIND1
C9
SERPINI
C5
C2
C1
ITIH3
Decreased plasma concentration during the acute phase response
Increased plasma concentration during the acute phase response

Figure S9.

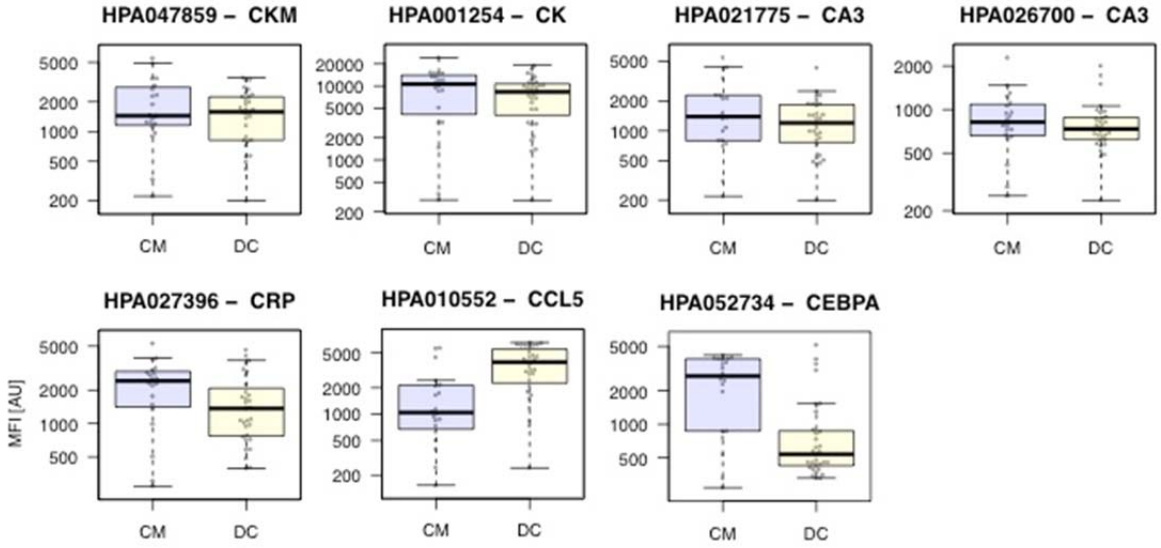
HPA047859 – CKM
HPA001254 – CK
HPA021775 – CA3
HPA026700 – CA3
HPA027396 – CRP
HPA010552 – CCL5
HPA052734 – CEBPA
MFI [AU]
CM
DC

Figure S10.

Supplementary Tables

	Protein	Antibody	p-value (Wilcoxon, Bonf. adj.)
UM vs SMA	IGFBP1	HPA046972	7,10E-13
	C3	HPA020432	2,60E-07
	VWF	HPA002082	6,15E-07
	BPGM	HPA016493	6,80E-07
	VWF	HPA001815	3,10E-05
UM vs CM	CA3	HPA021775	1,28E-16
	CA3*	HPA026700	6,86E-09
	BPGM	HPA016493	1,09E-08
	VWF	HPA002082	1,55E-08
	C3	HPA020432	1,60E-07
	MB	HPA003123	1,76E-07
	VWF	HPA001815	2,15E-06
	CK	HPA001254	1,81E-05
	IGFBP1	HPA046972	2,20E-05
SMA vs CM	CK	HPA001254	8,56E-10
	CA3	HPA021775	3,11E-08
	CA3*	HPA026700	2,87E-07

Table S1.

	Protein	Protein description	Antibody	AUC
UM vs SMA	**IGFBP1**	insulin-like growth factor binding protein 1	HPA04697	0,847
	VWF	von Willebrand factor	HPA00208	0,865
	HBA 1,2	hemoglobin, alpha 2, hemoglobin, alpha 1	HPA04378	0,870
UM vs CM	**CA3**	carbonic anhydrase III, muscle specific	HPA02177	0,891
	AGT	angiotensinogen (serpin peptidase inhibitor, clade A, 8)	HPA00155	0,917
	FBLN1	fibulin 1	HPA00161	0,935
	BPGM	2,3-bisphosphoglycerate mutase	HPA01649	0,950
	CA3*	carbonic anhydrase III, muscle specific	HPA02670	0,954
	MB	myoglobin	HPA00312	0,959
	IGFBP1	insulin-like growth factor binding protein 1	HPA04697	0,963
	ELANE	elastase, neutrophil expressed	HPA00118	0,972
	FURIN	furin (paired basic amino acid cleaving enzyme)	HPA00590	0,974
	CTSD	cathepsin D	HPA00300	0,975
	CCL17	chemokine (C-C motif) ligand 17	HPA04087	0,973
	GPT	glutamic-pyruvate transaminase	HPA03105	0,975
	CK	creatine kinase	HPA00125	0,975
	HSPG2	heparan sulfate proteoglycan 2	HPA01889	0,979
	ACTN2	actinin, alpha 2	HPA00831	0,979
	IGJ	immunoglobulin J polypeptide	HPA04413	0,979
	TNFSF13B	tumor necrosis factor (ligand) superfamily, member 13b	HPA03054	0,983
	C5	complement component 5	HPA02933	0,987
	F2	coagulation factor II (thrombin)	HPA00735	0,987
	VWF	von Willebrand factor	HPA00208	0,986
	TIE1	tyrosine kinase with immunoglobulin-like and EGF-like	HPA02743	0,986
	ADAMTS13	ADAM metallopeptidase with thrombospondin motif 1, 13	HPA04284	0,986
	PAFAH1B3	platelet-activating factor acetylhydrolase 1b	HPA03563	0,986
SMA vs CM	**CA3**	carbonic anhydrase III, muscle specific	HPA02177	0,783
	CK	creatine kinase	HPA00125	0,840
	IGFBP1	insulin-like growth factor binding protein 1	HPA04697	0,860
	ITGA2B	integrin, alpha 2b (antigen CD41)	HPA03117	0,866
	CTSD	cathepsin D	HPA00300	0,881
	SAA4*	serum amyloid A4, constitutive	HPA04868	0,900
	NGF	nerve growth factor (beta polypeptide)	HPA05029	0,903
	CALC A,B	calcitonin-related polypeptide beta, alpha	HPA04370	0,903
	FURIN	furin (paired basic amino acid cleaving enzyme)	HPA00590	0,911

* was excluded from verification cohort

Table S2.

Von Willebrand factor (VWF)	length	seq	
HPA002082	125aa	1379-1503	RITLLLMASQEPQRMSRNFVRYVQGLKKKKVIVIPVGIGPHA NLKQIRLIEKQAPENKAFVLSSVDELEQQRDEIVSYLCDLAPE APPPTLPPDMAQVTV GPGLLGVSTLGPKRNSMVLDVAFVL
HPA001815	125aa	1815-1939	ARSNRVTVFPIGIGDRYDAAQLRILAGPAGDSNVVKLQRIEDL PTMVTLGNSFLHKLCSGFVRICMDEDGNEKRPGDVWTLPDQ CHTVTCQPDGQTLLKSHRVNCDRGLRPSCPNSQSPVKVEKT
Carbonic anhydrase III (CA3)			
HPA021775	76 aa	14- 89	DHWHELFPNAKGENQSPVELHTKDIRHDPSLQPWSVSYDGG SAKTILNNG KTCRVVFDDTYDRSMLRGGPLPGPYR
HPA026700	71aa	190-260	YWTYQGSFTTPPCEECIVWLLLKEPMTVSSDQMAKLRSLLSS AENEPPVP LVSNWRPPQPINNRVVRASFK
Creatine kinase (CK)			
HPA001254 (CKB/M)	145aa	237-381	VISMQKGGNMKEVFTRFCTGLTQIETLFKSKDYEFMWNPHL GYILTCPSNLGTGLRAGVHIKLPNLGKHEKFSEVLKRLRLQKR GTGGVDTAAVGGVFDVSNADRLGFSEVELVQMVVDGVKLLI EMEQRLEQGQAIDDLMPAQK
HPA047859 (CKM)	24aa	1-24	MPFGNTHNKFKLNYKPEEEYPDLS

Table S3. Antibody-antigen properties.

Gene	Uniprot	HPA	Univariate hit	Multivariate hit
A1BG	P04217	HPA041687		
A2M	P01023	HPA002265		
ABCB7	O75027	HPA034982		
ACE2	Q9BYF1	HPA043894		
ACTN2	P35609	HPA008315		(x)
ADA	P00813	HPA001399	x	
ADA	P00813	HPA023884	x	
ADAMTS13, ADAMTS13.1	Q76LX8	HPA042844		(x)
ADM	P35318	HPA031806	x	
AGL	P35573	HPA028498		
AGT	P01019	HPA001557	x	x
AHSG	P02765	HPA001524		
AHSG	P02765	HPA001525		
AK5	Q9Y6K8	HPA019128		
ALB	P02768	HPA031025		
AMBP	P02760	HPA001497		
ANG	P03950	HPA036017		
ANG	P03950	HPA036018		
ANGPT1	Q15389	HPA018816		
ANGPT1	Q15389	HPA018793		
ANXA13	P27216	HPA018535		
ANXA13	P27216	HPA019569		
ANXA13	P27216	HPA019650		
ANXA5	P08758	HPA035330		
APOA1	P02647	HPA046715		
APOF	Q13790	HPA001902		
APOL1	O14791	HPA018885		
APOL5	Q9BWW9	HPA040968		
APP	P05067	HPA001462		
AREG, AREGB	P15514	HPA008720		
ARG2	P78540	HPA000663		
ARSB	P15848	HPA037770		
ARSB	P15848	HPA037771		
ASL	P04424	HPA016646		
ATRN	O75882	HPA008853		
AXL	P30530	HPA037422		
AZGP1	P25311	HPA012582		
B2M	P61769	HPA006361		
BASP1	P80723	HPA045218		
BCHE	P06276	HPA001560		
BCL6	P41182	HPA004899		
BDNF	P23560	HPA005774		
BMP1	P13497	HPA014572		
BMP2	P12643	HPA049966		
BMP3	P12645	HPA045344		
BMP7	P18075	HPA009264		
BMP7	P18075	HPA009158		
BPGM	P07738	HPA016493	x	x
BPGM	P07738	HPA016493	x	
BPGM	P07738	HPA028735		
C17orf57	Q8IY85	HPA021633		
C17orf57	Q8IY85	HPA026561		
C1S	P09871	HPA018852		
C3	P01024	HPA003563		
C3	P01024	HPA020432		
C4B, C4A	P0C0L4	HPA046356		
C4B, C4A	P0C0L4	HPA050103		
C4BPA	P04003	HPA000926		
C4BPA	P04003	HPA001578		
C5	P01031	HPA029339		(x)
C6	P13671	HPA043823		
C7	P10643	HPA001465		
C8A	P07357	HPA028217		
C8A	P07357	HPA028221		
C8B	P07358	HPA023694		
C9	P02748	HPA029577		
CA2	P00918	HPA001550		
CA3	P07451	HPA021775	x	x
CA3	P07451	HPA026700	x	x
CALCB, CALCA	P10092,	HPA043700		(x)
CAMP	P49913	HPA029874		
CCL1	P22362	HPA049861		
CCL11	P51671	HPA011652		
CCL14	Q16627	HPA030268		
CCL15	Q16663	HPA046429		
CCL16	O15467	HPA042909		
CCL17	Q92583	HPA040876		(x)
CCL18	P55774	HPA047485		

CCL19	Q99731	HPA026849		
CCL22	O00626	HPA046252		
CCL23	P55773	HPA042015		
CCL24	O00175	HPA035631		
CCL27	Q9Y4X3	HPA042918		
CCL28	Q9NRJ3	HPA046231		
CCL5	P13501	HPA010552	x	
CCL7	P80098	HPA045228		
CCL8	P80075	HPA050280		
CD14	P08571	HPA002127	x	
CD14	P08571	HPA001887	x	
CD27	P26842	HPA038936		
CD27	P26842	HPA038937		
CD33	P20138	HPA035832		
CD40	P25942	HPA031567		
CD40	P25942	HPA031568		
CD40LG	P29965	HPA045827		
CD44	P16070	HPA005785		
CD55	P08174	HPA002190		
CD55	P08174	HPA024386x		
CD59	P13987	HPA026494		
CD5L	O43866	HPA026432		
CD8B	P10966	HPA029164		
CD9	P21926	HPA005677		
CDH12	P55289	HPA006309		
CDH12	P55289	HPA006310		
CDH16	O75309	HPA036260		
CDH5	P33151	HPA030562		
CDH6	P55285	HPA007456		
CFB	P00751	HPA001817		
CFB	P00751	HPA001832		
CFH, CFHR1	P08603,	HPA038922		
CFI	P05156	HPA001143		
CKB	P12277	HPA001254	x	x
CLCF1	Q9UBD9	HPA042444		
CNDP1	Q96KN2	HPA008933		
CNTF	P26441	HPA019654		
COL18A1	P39060	HPA011025		
CP	P00450	HPA001834		
CPB2	Q96IY4	HPA004146		
CPN1	P15169	HPA040323		
CPN1	P15169	HPA040323x		
CPN2	P22792	HPA004732		
CRP	P02741	HPA027396	x	
CSF1	P09603	HPA022244	x	
CSF2	P04141	HPA048058		
CSF3	P09919	HPA001412		
CXCL1, CXCL3, CXCL2	P09341,	HPA043754		
CXCL10	P02778	HPA046579		
CXCL11	O14625	HPA042298		
CXCL16	Q9H2A7	HPA028972		
CXCL6	P80162	HPA043269		
DEFA1, DEFA1B, DEFA3	P59665,	HPA044693		
DEFB104B, DEFB104A	Q8WTQ1	HPA045292		
EDN1	P05305	HPA031977		
EDN1	P05305	HPA031978		
EDN3	P14138	HPA036618		
EGFR	P00533	HPA018530x		
ELANE	P08246	HPA001184		x
ENG	P17813	HPA011862		
EPB41L2	O43491	HPA005730		
EPB41L2	O43491	HPA006642	x	
EPO	P01588	HPA027572		
EPOR	P19235	HPA012110		
EPOR	P19235	HPA036320		
F10	P00742	HPA030629	x	
F11	P03951	HPA039808		
F12	P00748	HPA003825x		
F13A1	P00488	HPA001804		
F13B	P05160	HPA003827		
F2	P00734	HPA007359		(x)
F3	P13726	HPA049292		
F5	P12259	HPA002036		
F7	P08709	HPA004826		
F8	P00451	HPA000594		
F8	P00451	HPA000284		
F8	P00451	HPA000284		
F9	P00740	HPA000254		
FBLN1	P23142	HPA001612		
FBLN1	P23142	HPA001613	x	x
FGB	P02675	HPA001901		
FGG	P02679	HPA027529		

FIGF	O43915	HPA027342		
FKBP5	Q13451	HPA031092		
FKBP5	Q13451	HPA031093		
FLT1	P17948	HPA011740	x	
FN1	P02751	HPA027066		
FSTL3	O95633	HPA045378		
FTMT, FTH1	Q8N4E7,	HPA043650		
FURIN	P09958	HPA005905	x	x
G6PD	P11413	HPA000247		
G6PD	P11413	HPA000247		
G6PD	P11413	HPA000834		
GAL	P22466	HPA049864		
GC	P02774	HPA001526		
GDF5	P43026	HPA015648		
GP1BA	P07359	HPA013316		
GPT	P24298	HPA031059		(x)
GPT	P24298	HPA031060		
GPX1	P07203	HPA044758	x	
HABP2	Q14520	HPA021074	x	
HABP2	Q14520	HPA019518	x	
HBA2, HBA1	P69905	HPA043780		(x)
HBB, HBD, HBG1	P68871,	HPA043234		
HFE2	Q6ZVN8	HPA014472		
HGF	P14210	HPA040360		
HGF	P14210	HPA044088		
HIF1A	Q16665	HPA001275		
HIF1AN	Q9NWT6	HPA001179		
HIF1AN	Q9NWT6	HPA029260		
HIF3A	Q9Y2N7	HPA041141		
HMGB2, HMGB1	P09429,	HPA003506		
HMOX1	P09601	HPA000635		
HMOX2	P30519	HPA040611		
HP, HPR	P00738,	HPA047750		
HRG	P04196	HPA050269		
HSPG2	P98160	HPA018892		(x)
ICAM1	P05362	HPA004877		
IFNA21, IFNA4, IFNA7	P01568,	HPA047557		
IFNB1	P01574	HPA038795		
IFNB1	P01574	HPA038794		
IFNG	P01579	HPA049525		
IFNW1, IFNA21, IFNA4	P05000,	HPA045659		
IGFBP1	P08833	HPA046972	x	x
IGJ	P01591	HPA044132		(x)
IL11	P20809	HPA044955		
IL12A	P29459	HPA001886		
IL12B	P29460	HPA041100		
IL16	Q14005	HPA018467		
IL17A	Q16552	HPA045886		
IL17F	Q96PD4	HPA028770		
IL18	Q14116	HPA003980		
IL19	Q9UHD0	HPA049514		
IL1A	P01583	HPA030643		
IL1B	P01584	HPA044649		
IL20	Q9NYY1	HPA031387		
IL22	Q9GZX6	HPA023684		
IL23A	Q9NPF7	HPA001554		
IL24	Q13007	HPA008252		
IL28B, IL28A	Q8IZI9,	HPA043017		
IL29	Q8IU54	HPA014071		
IL2RA	P01589	HPA046738		
IL3	P08700	HPA030770		
IL4	P05112	HPA042270		
IL6R	P08887	HPA001411		
IL6R	P08887	HPA047592		
IL7	P13232	HPA019590	x	
IL8	P10145	HPA045822		
ITGA2B	P08514	HPA031170		(x)
ITGA2B	P08514	HPA031168		
ITGA2B	P08514	HPA031169		
ITGA3	P26006	HPA008572		
ITGA5	P08648	HPA002642		
ITGA6	P23229	HPA027585		
ITGAE	P38570	HPA036313		
ITGAV	P06756	HPA004856		
ITGB3	P05106	HPA027852		
ITIH1	P19827	HPA042049		
ITIH5	Q86UX2	HPA038304		
ITIH6	Q6UXX5	HPA001686		
KLKB1	P03952	HPA005634		
KNG1	P01042	HPA001645		
LBP	P18428	HPA001508	x	
LCN2	P80188	HPA002695		

LCP1	P13796	HPA019493	x	
LEP	P41159	HPA030721		
LEP	P41159	HPA030722		
LIF	P15018	HPA018844		
LRG1	P02750	HPA001888		
LRG1	P02750	HPA001889		
MASP1	P48740	HPA001617		
MASP1	P48740	HPA009641		
MASP2	O00187	HPA029314		
MASP2	O00187	HPA029313		
MB	P02144	HPA003123		x
MBL2	P11226	HPA002027		
MCAM	P43121	HPA008848		
MGP	P08493	HPA013949		
MIF	P14174	HPA003868		
MMP1	P03956	HPA007713		
MMP1	P03956	HPA031456		
MMP13	P45452	HPA036107		
MMP13	P45452	HPA036106		
MMP2	P08253	HPA001939	x	
MMP3	P08254	HPA007875x		
MMP7	P09237	HPA006991		
MMP8	P22894	HPA021221		
MMP8	P22894	HPA022935		
MMP9	P14780	HPA001238		
MMP9	P14780	HPA001238		
MPL	P40238	HPA007619		
MPO	P05164	HPA021147		
MSTN	O14793	HPA018534		
MSTN	O14793	HPA021681x		
NAIP	Q13075	HPA047000		
NAIP	Q13075	HPA042438		
NAIP	Q13075	HPA050102		
NCAM1	P13591	HPA039835		
NCAM2	O15394	HPA030900		
NEFM	P07197	HPA023138		
NEFM	P07197	HPA022845	x	
NGF	P01138	HPA050298		(x)
NOS1	P29475	HPA043350		
NOS2	P35228	HPA038086		
NOS2	P35228	HPA038087		
NOS3	P29474	HPA040212		
NRP1	O14786	HPA002880		
NTF3	P20783	HPA032000		
ORM1, ORM2	P02763,	HPA046438		
ORM1, ORM2	P02763,	HPA047725	x	
OSM	P13725	HPA029814		
PAFAH1B1	P43034	HPA020036		
PAFAH1B3	Q15102	HPA035639		(x)
PDGFA	P04085	HPA045273		
PDGFB	P01127	HPA011972		
PF4V1, PF4	P10720,	HPA043455		
PIGR	P01833	HPA006154		
PLA2G1B	P04054	HPA047822		
PLAT	P00750	HPA003412		
PLAU	P00749	HPA008719		
PLG	P00747,	HPA021602		
POMC	P01189	HPA046135		
POSTN	Q15063	HPA012306		
PPBP	P02775	HPA008354		
PPBP	P02775	HPA008354		
PROC	P04070	HPA005550		
PROS1	P07225	HPA007724		
PROS1	P07225	HPA023974		
PROZ	P22891	HPA016503		
PTGDS	P41222	HPA004938		
RBP4	P02753	HPA001641		
REG3G, REG3A	Q6UW15,	HPA048334		
RELN	P78509	HPA046512		
REN	P00797	HPA005131		
CTSD	P07339	HPA003001		(x)
S100A1	P23297	HPA006462		
S100A4	P26447	HPA007973		
S100A7A, S100A7	Q86SG5,	HPA006997		
S100A8	P05109	HPA024372		
S100A9	P06702	HPA004193		
S100B	P04271	HPA015277		
SAA4	P35542	HPA048680		(x)
SDC1	P18827	HPA006185		
SEBOX	Q9HB31	HPA045689		
SELP	P16109	HPA002655		
SERPINA1	P01009	HPA001292		

SERPINA3	P01011	HPA000893	x	
SERPINA3	P01011	HPA002560	x	
SERPINA6	P08185	HPA017864		
SERPINC1	P01008	HPA001816		
SERPINC1	P01008	HPA024007		
SERPINE1	P05121	HPA001539		
SERPINE1	P05121	HPA024527		
SERPINE2	P07093	HPA000277		
SERPINE2	P07093	HPA000277		
SERPINF1	P36955	HPA005825		
SERPINF2	P08697	HPA001885		
SLC12A3	P55017	HPA028748	x	
SLC40A1	Q9NP59	HPA011754		
SOD1	P00441	HPA001401		
SPP1	P10451	HPA005562		
SPP1	P10451	HPA027540		
TF	P02787	HPA001527		
TFPI	P10646	HPA005575		
TFR2	Q9UP52	HPA011937		
TFRC	P02786	HPA028598		
TGFA	P01135	HPA042297		
TGFB2	P61812	HPA006373		
TGFB2	P61812	HPA049818		
TGFB3	P10600	HPA001129		
TGFBI	Q15582	HPA008612		
THPO	P40225	HPA042965		
THPO	P40225	HPA048828		
TIE1	P35590	HPA007243		
TIE1	P35590	HPA027432		(x)
TIMP2	P16035	HPA001764		
TIMP2	P16035	HPA049145		
TIMP3	P35625	HPA001139		
TLR9	Q9NR96	HPA004731		
TNFAIP1	Q13829	HPA013333		
TNFAIP1	Q13829	HPA014641		
TNFRSF1A	P19438	HPA019119		
TNFRSF1B	P20333	HPA004796	x	
TNFRSF8	P28908	HPA014720		
TNFSF11	O14788	HPA008128		
TNFSF13B	Q9Y275	HPA030546		(x)
TTR	P02766	HPA005150		
UTS2	O95399	HPA017000		
VCAM1	P19320	HPA001618	x	
VCAM1	P19320	HPA034796	x	
VEGFB	P49765	HPA044361		
VWF	P04275	HPA001815	x	
VWF	P04275	HPA002082	x	x
XCL2, XCL1	Q9UBD3,	HPA047690		

Table S4.

Methods S1

Clinical data and sample collection. A 2.5 ml blood sample was obtained from each participant in an EDTA blood collection tube for subsequent plasma separation. Blood samples were kept on ice and transferred to the central malaria laboratory. Plasma for this study was harvested by centrifugation (1000 *g*, 10 minutes), aliquoted and frozen at -80°C no later than 4 hours following collection. The total of freeze/thaw cycles was limited and did not exceed 3 times during the entire study.

Biotinylation of plasma samples. Biotinylation was performed as previously described [1] (refer to Supplementary Methods). Briefly, plasma samples were diluted using a liquid handler (SELMA, CyBio). Primary amino groups of plasma proteins were labeled using N-hydroxysuccinimide ester-biotin with a polyethylene oxide spacer (NHS-PEO4-Biotin, Pierce) as biotinylation reagent following the manufacturer's instructions. After incubation for 2 h, the reaction was stopped by the addition of 1 M Tris–HCl, pH 8.0 and samples were stored at −20°C. Two samples of the discovery cohort and four samples of the verification cohort had to be removed due to technical failure.

Quality assessment of suspension bead-array. To analyze the technical variation of the array, the initial screening using the 'targeted array' including 356 samples and 384 antibodies was reproduced in an independent experiment. The median coefficient of variation (CV) of sample replicates (n=12) within one experiment (intra-assay) was 5.5% for normalized data (Fig. S1A). To evaluate the inter-assay variation, the relative intensities between the two independent experiments were compared (Fig. S1B). The sample-wise median correlation coefficient was 0.992 ranging from 0.94 to 0.99. To assess the reproducibility also antibody-wise, the relative intensities of each antibody were compared in the two experiments. The correlation coefficients of antibodies ranged from 0.45 to 0.99 with a median of 0.89. Patient- and antibody-wise correlation coefficients were additionally determined for the 24 duplicated patient samples in discovery and validation cohort with the top 30 proteins. The median correlation coefficient for antibody-wise correlations was 0.67 and for sample-wise correlations 0.64 due to the low number of samples (Fig. S1C).
In general, many substantial differences ($p < 0.001$) in protein profiles were found between the patient groups when utilizing the 'targeted array'. In order to confirm that the observed

differences were specific to the pre-selected set of proteins in the 'targeted array', profiling with 'random arrays' was conducted. To obtain an overview of the observed differences in the 'targeted array' and the 'random arrays' principal component analysis (PCA) was performed, which provides a visualization tool for information-rich data by reducing the dimensionality. By projecting the data into the first few principal components, separations between disease groups can be observed dependent on the variables (proteins). Interestingly, the PCA of the 'targeted array' indicated a more spread separation by the proteins contained in this array compared to the 'random array' (Fig. S2A). Hence, the observed large differences were specific to the selected antibodies.

Immunohistochemistry. Immunohistochemical analysis was performed on healthy adult Human tissues as described before according to the Human Protein Atlas (HPA) standard operating procedures [2]. All incubations were performed at room temperature and reagents were from Thermo Fisher Scientific, unless specified. Briefly, prior to immunostaining, deparaffinization and hydration in xylene and graded ethanol to distilled water using a Leica Autostainer XL (Leica Biosystems, Wetzlar, Germany) were performed. Endogeneous peroxidase was blocked using 0.3 % H_2O_2 in 95% ethanol for 5 minutes. Pressure boiling (Decloaking chamber, Biocare Medical, Walnut Creek, CA) with retrieval buffer pH6 for 4 minutes at 125°C was carried out to perform heat induced epitope retrieval (HIER). After HIER, slides were allowed to cool to 90°C. Immunohistochemistry was performed using an Autostainer 480 (Thermo Fisher Scientific, Waltham, MA, USA). Between procedures described below, sections were washed in wash buffer twice. To block cross reactivity, incubation with UV block for 5 minutes was performed. Rabbit polyclonal antibodies affinity-purified using the antigen as affinity-ligand [3] and secondary labeled horse radish peroxidase-polymer were incubated for 30 minutes, respectively. Thereafter 3,3´-Diaminobenzidine (DAB) was used for detection for 10 minutes. Counterstaining was performed using hematoxylin (Histolab, Järfälla, Sweden) for 5 minutes and then the slides were rinsed in tap water and lithium carbonate water, diluted 1:5 from saturated solution, in total 10 min. Finally, the slides were dehydrated in graded ethanol. Stained slides were scanned using an automated high-resolution slide scanner (Aperio Technologies, Vista, CA, USA).

Self-organizing tree algorithm (SOTA) analysis. The SOTA algorithm combines the advantages of both hierarchical clustering and Self-Organizing Maps (SOM). Briefly, it picks

a node with the largest diversity and splits it into two nodes[4]. The tree was allowed to grow for 4 cycles. To visualize the high dimensional array data set we applied principal components analysis (PCA) using the R function prcomp[5-7]. Thereby, the dimensionality of the data set was reduced while maintaining as much variance as possible. Calculation is done by a singular value decomposition of the scaled and centered data matrix.

Multivariate analysis. Several logistic regression models with different variables (sex, age proteins) were fitted. In order to achieve a robust result, in each model hundred fits with different random seeds were performed. Based on the resulting λ_1-value in each fit, the average λ_1 was used to fit the model. Because the variables age and sex did not provide large contribution to the classification, the analysis was continued using only proteins as variable for classification. The resulting protein panels as well as the corresponding area under the ROC curve (AUC) of each model is presented.

L1-penalized logistic regression model

Multiclass classification and at the same time performing feature (e.g., proteins) selections commonly faced in many biological applications is not a trivial problem. One way to deal with multiclass (i.e., UM, SMA and CM) classification is to decompose the classification into several binary classification tasks (one-vs.-one). Then, on each binary classification, binary classifiers are obtained using a binary classification method, i.e., L_1 penalized-logistic regression.

Logistic regression is a supervised method for binary classification [8]. Because it is a simple, flexible and straightforward model that is easy to extend, the extensions of logistic regression have been widely used in genomics and proteomics research [9, 10].

In high-dimensional datasets such as an array, where usually variables are in similar or higher numbers than observations are available, and where the variables are correlated (multicollinearity), the classical logistic regression would perform badly and provide inaccurate estimates. It could result in a perfect fit to the data with no bias and high variance, which would lead to inaccurate predictions. In order to prevent this problem, a penalty for complexity in the model was introduced.

In our case, *yi* is an array of two malaria disease subtypes (i.e., cerebral malaria (CM), severe malarial anemia (SMA), or uncomplicated malaria (UM)), and *xj* is the intensity level of the *j*th protein. We can fit the following logistic model:

$$\log it(p(x_i)) = \beta_0 + \sum_{j=1}^{m} \beta_j x_j$$

where p(x) is the probability of success (i.e., y = 1) given x. To fit this model, the following log-likelihood had to be optimized:

$$\ell(\beta) = \sum_{j=1}^{n} \{y_i \log(p(x_i)) + (1 - y_i) \log(1 - p(x_i))\}$$

To penalize logistic regression, we can impose a penalty as defined in the following penalized log-likelihood:

$$\ell^*(\beta) = \ell(\beta) - \lambda J(\theta)$$

where $J(\theta)$ is a penalty function. There are several penalty functions being proposed, and in this study we implement the ℓ1 penalization proposed by Tibshirani [11] and known as Lasso. The ℓ1 penalization use

$$J(\theta) = \sum_{i=1}^{n} \|\beta_i\|$$

as the penalty function. The Lasso shrinks all regression coefficients β toward zero and set some of them to zero. Hence, it performs parameter estimation and variable selection at the same time. For a defined value of λ, the challenge is to optimize the penalized log-likelihood. Goeman [12] proposed the *full gradient* algorithm for maximizing Lasso-penalized log-likelihood. The choice of the tuning parameter λ is crucial. Since the *full gradient* algorithm finds the estimates of regression coefficients for a fixed value of λ, the optimal value of λ is found by a cross-validation procedure. In this procedure, cross-validated partial log-likelihood for a range of λ was calculated and the λ value, which gives the maximum log-likelihood is selected using Brent's algorithm [13]. These algorithm and procedures are implemented in an R package called penalized [12].

Note that the sample partitioning in the cross-validation procedure are performed randomly, which can lead to slightly different λ values for different random seed numbers. To obtain the more reliable λ, 100 cross-validations are performed with different random seed numbers and the obtained (λ1, λ2, ..., λ100) are averaged ($\bar{\lambda}$). The final ℓ1-penalized model is then fitted based on the $\bar{\lambda}$.

References

1. Neiman M, Hedberg JJ, Donnes PR, et al. Plasma profiling reveals human fibulin-1 as candidate marker for renal impairment. *J Proteome Res* 2011; **10**(11): 4925-34.
2. Kampf C, Olsson I, Ryberg U, Sjostedt E, Ponten F. Production of tissue microarrays, immunohistochemistry staining and digitalization within the human protein atlas. *Journal of visualized experiments : JoVE* 2012; (63).
3. Nilsson P, Paavilainen L, Larsson K, et al. Towards a human proteome atlas: high-throughput generation of mono-specific antibodies for tissue profiling. *Proteomics* 2005; **5**(17): 4327-37.
4. Herrero J, Valencia A, Dopazo J. A hierarchical unsupervised growing neural network for clustering gene expression patterns. *Bioinformatics* 2001; **17**(2): 126-36.
5. Venables WNaBDR. Modern Applied Statistics with S: Springer-Verlag; 2002.
6. Mardia KV, J. T. Kent, and J. M. Bibby. Multivariate Analysis: London: Academic Press; 1979.
7. Becker RA, Chambers, J. M. and Wilks, A. R. The New S Language: Wadsworth & Brooks/Cole; 1988.
8. Hosmer DW, Lemeshow, S. Applied Logistic Regression. New York, NY: Wiley; 1989.
9. Liao JG, Chin KV. Logistic regression for disease classification using microarray data: model selection in a large p and small n case. *Bioinformatics* 2007; **23**(15): 1945-51.
10. Sun H, Wang S. Penalized logistic regression for high-dimensional DNA methylation data with case-control studies. *Bioinformatics* 2012; **28**(10): 1368-75.
11. Tibshirani R. Regression shrinkage and selection via the lasso: a retrospective. *J R Stat Soc B* 2011; **73**: 273-82.
12. Goeman JJ. L1 penalized estimation in the Cox proportional hazards model. *Biometrical journal Biometrische Zeitschrift* 2010; **52**(1): 70-84.
13. Brent RP. Algorithms for Minimization without Derivatives: Englewood Cliffs: Prentice-Hall; 1973.